

Analytical and numerical study of a curved planar waveguide with combined Dirichlet and Neumann boundary conditions in a uniform magnetic field

O. Olendski*

Atomic and Molecular Engineering Laboratory, Belarusian State University, Skarina Avenue 4, Minsk 220050, Belarus

L. Mikhailovska

Department of Higher Mathematics, Military Academy, Minsk 220057, Belarus

(Received 3 June 2007; revised manuscript received 3 April 2008; published 2 May 2008)

A model of a thin straight strip with a uniformly curved section and with different uniform boundary conditions on the opposite edges subjected to the homogeneous magnetic field \mathbf{B} is theoretically analyzed within the framework of the linear Schrödinger equation and is applied to the study of the processes in the bent magnetic multilayers and superconducting films. In particular, for the inner Dirichlet and outer Neumann boundaries, it is shown that bend-induced enhancement of the superconductivity survives in the magnetic field with the order parameter $\Psi(\mathbf{r})$ being pushed stronger and stronger to the Neumann surface with increasing B and, simultaneously, the area where the nucleation of the superconductivity takes place is spread more and more in the straight arms. Various magnetotransport properties of the film such as interference blockade of the supercurrent flow at some special field-dependent temperatures are also discussed with special attention being paid to the formation and evolution of the vortices, which appear as a result of the bend-induced interaction between the different subbands; it is shown, in particular, that the number of vortices decreases with the field and some of them transform into the antivortices. A proof of the very close analogy between two kinds of strips, (1) pure Dirichlet condition on both edges and (2) inner Dirichlet and outer Neumann requirements, derived earlier for $B=0$ is extended to the case of nonzero fields.

DOI: [10.1103/PhysRevB.77.174405](https://doi.org/10.1103/PhysRevB.77.174405)

PACS number(s): 75.70.Ak, 74.20.De, 74.78.-w, 74.25.Dw

I. INTRODUCTION

Study of magnetic multilayers in recent years¹ has brought a lot of new and fascinating physics, such as interlayer exchange coupling,²⁻⁶ giant magnetoresistance,^{6,7} or current-driven switching of magnetic layers.⁸⁻¹⁰ The underlying physical mechanism of these phenomena is the spin-dependent reflectivity at the magnetic/nonmagnetic interfaces,^{6,7} which, in turn, stems from the fact that the spin-up electrons in the ferromagnetic layer have their band aligned with the counterpart in the nonmagnetic interlayer, while the spin-down bands are shifted upward on the energy scale and, accordingly, the good match with the bands in the spacer is lost.⁶ As a result, an electron with a spin parallel to the magnetic moment of the ferromagnet almost freely traverses the magnetic/nonmagnetic boundary, and a particle with the opposite spin is reflected from it.⁶

So far, the properties of only the straight magnetic multilayers have been under consideration. One of the latest literature surveys on spin transport in magnetic nanostructures is provided in Ref. 11. In the present research, we theoretically discuss the magnetotransport and electronic properties of the bent magnetic layers. For doing this, we model the transverse potential profile “seen” by the longitudinally itinerant electrons as a potential well.^{12,13} For the ferromagnetic arrangement, the electron with a spin antiparallel to the magnetization of the magnetic layers will be trapped in the potential well inside the nonmagnetic spacer if the corresponding spin directions are fully occupied in the magnetic strips.⁶ Thus, to a good first approximation, its transverse motion can be described by the infinitely deep potential well with Dirichlet boundary conditions;^{6,14} namely, its wave function

vanishes at the magnetic/nonmagnetic boundaries. In turn, for the antiferromagnetic ordering, when the magnetizations of the adjacent magnetic layers point in the opposite directions parallel to the interfaces, electron transverse motion for both spins can be reasonably well described by the potential well with the Dirichlet boundary condition on one side and the Neumann requirement (vanishing of the spatial derivative of the wave function in the transverse direction) on the opposite edge.¹⁴ To exemplify this, one can imagine the situation when the transverse potential created by the two straight adjacent layers of widths d and s effectively binds an electron with a mass m inside them, but there exists a potential step V_0 between neighboring layers due to their different polarizations [see Fig. 1(a)]. Then, the transverse propagation thresholds E_n of such a system in the absence of the magnetic fields are determined from the following equation:

$$\sqrt{1 + \frac{V_0}{E_n}} \sin(\pi\sqrt{E_n}) \cos(\pi\sqrt{E_n + V_0}s) + \cos(\pi\sqrt{E_n}) \sin(\pi\sqrt{E_n + V_0}s) = 0, \quad (1)$$

where the distances are measured in units of d and the energies are in units of ground-state energy $\pi^2\hbar^2/(2md^2)$ of the infinitely deep Dirichlet quantum well of width d . Analysis of Eq. (1) shows that for $V_0=1/4(1/s^2-1)$, the fundamental propagation threshold for all $s \leq 1$ coincides with that for the Dirichlet–Neumann strip, $E_0=1/4$. In addition, for quite small s , other low thresholds E_n are very close to the energies $(n+1/2)^2$,

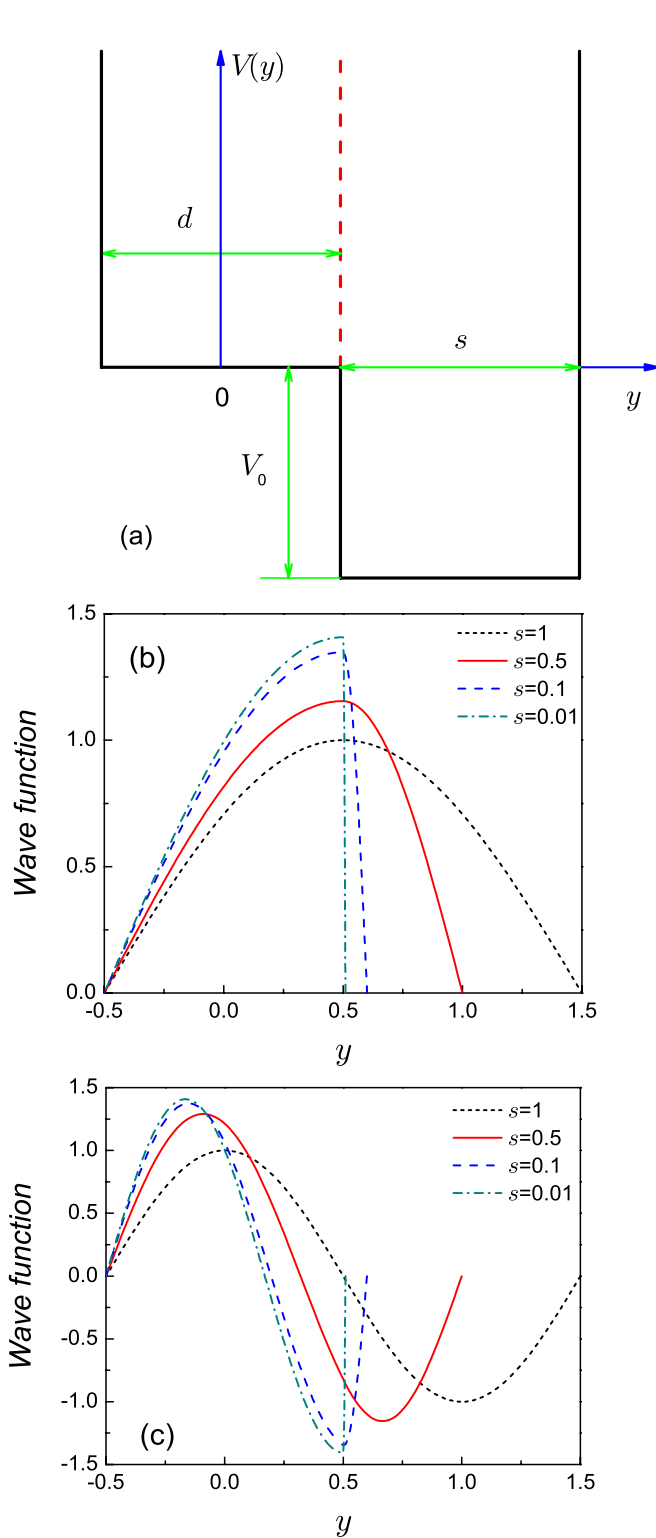


FIG. 1. (Color online) (a) Transverse potential profile of two magnetic layers with widths d and s . Energy gap between the layers is V_0 . Origin of the coordinate system coincides with the middle of the left well. The dashed line shows a boundary between the two layers. (b) Wave functions of the lowest state ($n=0$) for the normalized gap $V_0=1/4(1/s^2-1)$ and several normalized lengths s . (c) The same as in panel (b), but for the second propagation threshold ($n=1$).

$$\lim_{s \rightarrow 0} E_n|_{V_0=(1/s^2-1)/4} = (n+1/2)^2, \quad n=1,2,\dots, \quad (2)$$

which are characteristic for the Dirichlet–Neumann quantum well. Corresponding wave functions for the two lowest n and several s are shown in panels (b) and (c) of Fig. 1. It is seen that for a small s , one can model the system as having mixed boundary conditions at $y=\pm 1/2$. This is especially true for the fundamental propagation threshold when the derivative of the wave function identically vanishes at $y=1/2$ for any s . We will return to a more quantitative analysis of this situation later in the text. In other words, under the special choice of the parameters, it is possible to describe the magnetic system as having a combination of Dirichlet and Neumann requirements. We note in passing that the electrons can also be trapped in the magnetic layer, say, for Fe/Cr(100) structures.¹⁵ In this case, there is no substantial difference between the minority-spin-band structure of the Fe and the Cr band structure, while the majority-spin bands of Fe are located below the Cr bands. As a result, majority-spin electrons face potential barriers at the surfaces, while minority-spin electrons freely pass through them. An even more general situation is possible when nonmagnetic spacers are the quantum well for one spin projection and the potential barrier for the opposite spin direction.⁴

In other words, spin-dependent reflectivity at the interfaces⁶ is described in our model by the different boundary conditions of the corresponding edges of the channel. In addition, our structure contains a uniform finite bend and is subjected to the homogeneous in-plane magnetic field \mathbf{B} being perpendicular to the electron longitudinal motion. We disregard the magnetic field influence on the spin of the electrons in the magnetic layers and, thus, field-induced transition from the antiferromagnetic to the ferromagnetic state is suppressed in our model. Quantum-size effects in the transverse direction lead to the quantized two-probe conductance along the duct.^{16,17} We note that the model of the waveguide with the different boundary conditions is applicable also in other areas of physics; for example, it describes continental shelf waves¹⁸ or electromagnetic wave propagation between the earth and the ionosphere.^{19,20} In solid-state physics, the same quantization of the transverse momenta takes place in the transmission of massless Dirac fermions through an ideal strip of graphene.²¹ A similar situation that will be our second primary target emerges also in the superconductivity. Namely, from the phenomenological theory of superconductivity,²² it is known that the behavior of the order parameter $\Psi(\mathbf{r})$ near the transition point is well described by the linearized Ginsburg–Landau (GL) equation,^{23,24}

$$\frac{1}{2m}(-i\hbar\nabla + q\mathbf{A})^2\Psi(\mathbf{r}) = -\alpha\Psi(\mathbf{r}). \quad (3)$$

Here, $\mathbf{B}=\nabla\times\mathbf{A}$ is the external magnetic field applied to the superconductor, where \mathbf{A} is corresponding vector potential; $q=2e$, where e is the absolute value of the electronic charge; and $-\alpha=[\hbar^2/2m\xi^2(0)](1-T/T_c)$ is the GL parameter where T is the actual temperature of the superconducting material, T_c is the bulk critical temperature at zero magnetic field, and $\xi(0)$ represents the zero-temperature coherence length. Com-

paring Eq. (3) to the usual Schrödinger equation,²⁵ one sees their complete analogy; namely, Eq. (3) describes the wave function $\Psi(\mathbf{r})$ of a particle of negative charge $-2e$ and mass m moving with a total energy of

$$E = \frac{\hbar^2}{2m\xi^2(0)} \left(1 - \frac{T}{T_c} \right), \quad (4)$$

in the magnetic field \mathbf{B} . This correspondence was widely used for the investigation of the superconducting properties near the phase boundary.^{23,24} In the GL theory, Eq. (3) is accompanied by the expression for the supercurrent density \mathbf{j} ,

$$\mathbf{j} = -i \frac{q\hbar}{2m} [\Psi \nabla \Psi^* - \Psi^* \nabla \Psi] - \frac{q^2}{m} \mathbf{A} |\Psi|^2. \quad (5)$$

When one considers spatially confined superconducting samples, it is necessary to take into account the boundary condition for the order parameter Ψ ,^{23,26}

$$\mathbf{n} \left(\nabla + i \frac{q}{\hbar} \mathbf{A} \right) \Psi|_{\mathcal{L}} = \frac{1}{\Lambda} \Psi|_{\mathcal{L}}, \quad (6)$$

where \mathbf{n} is a unit vector normal to the superconductor surface \mathcal{L} . Extrapolation length Λ in Eq. (6) can take positive as well as negative values. Physically, the value of $1/\Lambda$ that is equal to zero corresponds to the superconductor/vacuum or superconductor/insulator surface,^{22–24} while its positive magnitude describes the processes taking place at the superconductor-normal metal interface.^{23,24} In the case of superconductor/ferromagnet interface, the length Λ can take very large values, which means a suppression of superconductivity. In turn, negative values of Λ correspond to the border with the superconductor with the higher critical temperature,²⁷ which physically means enhancement of the surface superconductivity. Since the surface-to-volume ratio for the mesoscopic superconductors is not negligible as is the case for the bulk material, the boundary condition [Eq. (6)] is indispensable in defining the “energy” spectrum $-\alpha$ and other properties, such as magnetization, of the finite-sized superconductors. Theoretical predictions based on the solutions of Eqs. (3) and (6) (Ref. 28–35) are in good agreement with the experimental measurements^{36–38} (see Ref. 39 for more references).

One of the structures wherein the boundary effects are crucial in defining sample properties is the superconducting film.^{40,41} Quantum-size effects were shown to drastically modify the properties of superconductors. In particular, recent technological advances allowed physicists to grow ultrathin lead films on a silicon substrate and to demonstrate that superconducting transition temperature oscillates as a function of the film thickness.⁴²

In the present paper, within the framework of Eqs. (3) and (5), we study the properties of the curved magnetic or superconducting film in the in-plane uniform magnetic field \mathbf{B} . In our model, opposite walls of the strip impose either identical or different boundary conditions on the wave function (for magnetic materials) or the order parameter (for superconductors) Ψ . Under the selected choice of the gauge for the vector potential \mathbf{A} , as a result of its orientation to the con-

fining surfaces, it drops out from the boundary condition [Eq. (6)], which simplifies to

$$\nabla_n \Psi = \frac{1}{\Lambda} \Psi|_{\mathcal{L}}. \quad (7)$$

Below, for the extrapolation length Λ , we adopt two limiting cases; namely, on each of the confining walls of the strip, it can be either zero (Dirichlet requirement) or infinity (Neumann boundary condition). In addition to the magnetic layer structures discussed above, such a configuration can be fabricated by sandwiching the superconducting film between the insulator and the ferromagnet. Recently, the properties of a thin mesoscopic superconducting ring with different inner and outer extrapolation lengths were calculated.⁴³ Here, a few notes on the field-free curved waveguides are in order. Historically, early hints^{44,45} on the ability of the bent waveguide with Dirichlet boundary conditions to trap the wave inside the curved section were rigorously proved theoretically^{46–48} and were confirmed experimentally.⁴⁹ An extra space in the bend presents a shelter where the charged particles can dwell with their momenta smaller than the cut-off momentum of the lowest subband. Interference of the discrete level split off by the bend from the higher lying subband, with the continuum states of the lower mode, also drastically modifies the transport properties of the duct, leading to a steep dip on the conductance versus energy dependence.^{50,51} Recent theoretical studies discovered that the curved duct with the inner Dirichlet and outer Neumann requirements on the strip mimics the behavior of the Dirichlet film;^{18,52–54} in particular, it leads too to the bound state below the essential spectrum of the straight waveguide. In terms of the GL theory, it means, according to Eq. (4), an increased critical temperature of the bent strip compared to that of its straight counterpart. Thus, a suppression of the superconductivity caused by the introduction of the Dirichlet edge is partially compensated by the bending in the appropriate direction. A similar geometry-induced enhancement of the superconductivity was recently predicted for the cylinder and the sphere with the negative extrapolation length.⁵⁵ No bound state exists for the curved Neumann strip when the continuous spectrum covers all non-negative energy axis. Accordingly, in this case, the bend, as it follows from Eq. (4), does not change the critical temperature of the sample. Note also that curved planar waveguides possess a lot of interesting physics related to the Josephson transmission lines.^{56,57}

A brief survey of the theoretical and experimental research on the bent waveguides with Dirichlet boundary condition in the external magnetic field is given in Ref. 58. In addition to the literature cited therein, here, we want to mention recent calculations of the conductance of quasiparticles in an L-shaped bent quantum waveguide in an inhomogeneous magnetic field⁵⁹ when a semiconductor/superconductor junction at the exit arm was modeled by the introduction of δ -scattering potential. Andreev reflection⁶⁰ was shown to strongly influence the conductance of the structure.

In our approach to the theoretical investigation of the curved magnetic or superconducting strip in the external ho-

homogeneous magnetic field, we employ the same method used in the previous study of the bent semiconductor channel;⁵⁸ namely, in each part of the waveguide, we find an analytical solution of Eq. (3) and match them at the junctions between the curved section and the straight arms. It allows us to find the bound-state dependence on the magnetic field, which, in the case of superconductors, corresponds to the T_c - B phase boundary. The results of the bound-state analysis are equally valid both for the magnetic materials and the superconductors. We also calculate transport properties of the film; in particular, for temperatures below the critical one, we calculate transmission of the bend as a function of T . In addition, geometry-induced vortices present even at $B=0$ are shown to dramatically change for nonzero fields; in particular, for small and moderate magnetic intensities, the vortices in the straight arms near the junctions transform into the *antivortices* that correspond to the interference of the edge currents flowing along the opposite walls of the strip.

The paper is organized as follows: In Sec. II, our model is presented and a necessary formulation of our method is given. Section III is devoted to the presentation and detailed physical interpretation of the calculated results. Summary of the research is provided in Sec. IV.

II. MODEL AND FORMULATION

The structure we consider is schematically shown in Fig. 2. Infinitely long magnetic or superconducting strip of constant width d contains a uniformly curved section with an inner radius ρ_0 and an angle ϕ_0 . A uniform magnetic field \mathbf{B} is applied in the positive z direction. On each of the film sides, we impose a uniform boundary condition—either the Dirichlet or Neumann one. For brevity, a case when a Dirichlet (Neumann) condition is on the inner wall of the strip and the other condition on the outer side will be called a DN (ND) case below. Accordingly, the situation with the pure Dirichlet (Neumann) conditions on both sides of the channel is referred to as a DD (NN) configuration. From the geometry of the system, it directly follows that the inversion of the magnetic field is equivalent to the change from the up- to down-turn configuration with the previous direction of \mathbf{B} . Since from the corresponding calculations for the semiconductor channel it is known that, generally, up- and down-turn bends differently behave in the magnetic field,^{61,62} both of these configurations are shown in Fig. 2 and analyzed later in the text. We will look for the solution of Eq. (3) in terms of the energy E , which is more relevant for the ferromagnetic channel, switching, if necessary, to the temperature T of the superconductor, according to Eq. (4). Accordingly, our lexicon below will include interchangeable usage of both ferromagnetic and superconducting terms, and the results will be equally applicable to both of these materials, if not explicitly stated otherwise. It is assumed that a strip width along the z axis is much smaller than the penetration length λ of the superconductor, which means a uniform distribution of the field in this direction. Accordingly, the z dependence drops out from Eq. (3) and the problem becomes strictly two dimensional. Similarly, the homogeneous magnitude of \mathbf{B} inside the strip in the x and y directions is satisfied for $d \lesssim \lambda$. In

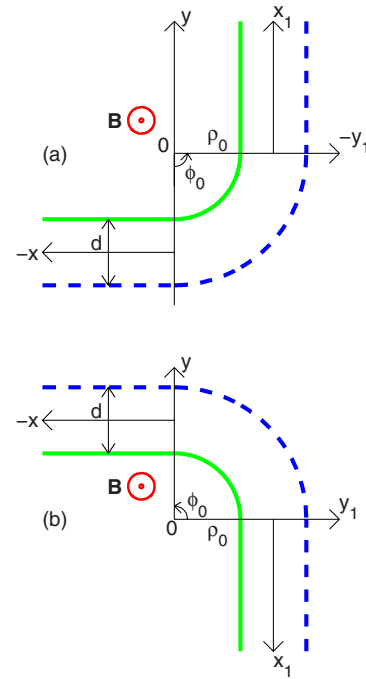


FIG. 2. (Color online) Schematic of the (a) up-turn and (b) down-turn curved magnetic or superconducting film in uniform magnetic field \mathbf{B} pointing in the positive z direction. The waveguide width is d and the bend angle and inner radius are ϕ_0 and ρ_0 , respectively. The inner (thick solid line) and outer (dashed line) surfaces of the duct support uniform boundary conditions that might be different on the opposite walls. The origin of the polar coordinate system (ρ, ϕ) coincides with the center of the bend. For case (a), the polar axis is a vertical junction of the straight and curved parts, while for case (b), it is the junction with the right straight channel. The curved arrows show the direction in which the azimuthal angle ϕ grows. The local Cartesian coordinate systems (x, y) and (x_1, y_1) for the straight arms are also shown. Their origins coincide with the middle of the corresponding junction with the bent part.

addition to the mentioned above units of distance and energy, we will measure all momenta in units of \hbar/d , magnetic fields in units of $\hbar/(qd^2)$, time in units of $2md^2/(\pi^2\hbar)$, velocity in units of $\hbar/(md)$, conductance in units of q^2/h , magnetic flux in units of h/q , and two-dimensional current density in units of $q\hbar/(md^3)$, where $q=e$ for the ferromagnetic layer and $q=2e$ for the superconductor.

In each part of the waveguide, a corresponding solution of Eq. (3) can be expressed in the analytical form. For example, in the straight arm to the left of the bend, it is convenient to choose the local Landau gauge for the vector potential $\mathbf{A}=(-yB, 0)$. Then, a total solution of Eq. (3) in this region is written as

$$\Psi(x, y) = \sum_{n=1}^{\infty} [C_n \chi_{p_n^{(+)}}(y) e^{ip_n^{(+)}x} + D_n \chi_{-p_n^{(-)}}(y) e^{-ip_n^{(-)}x}], \quad (8)$$

where transverse functions $\chi_{p_n}(y)$ satisfy either the Dirichlet or the Neumann boundary condition at the edges $y = \pm 1/2$. The first sum in Eq. (8) describes the waves incident on the bend, with a second term being a set of reflected (for the real

p_n) or localized near it (for the purely imaginary p_n) modes. Complex amplitudes C_n and D_n define the relative contribution of the n th subband into the total supercurrent. Properties of the functions $\chi_{p_n}(y)$ and the corresponding wave vectors p_n for the DD case were analyzed in detail in Refs. 58, 61, 63, and 64, and for any other configuration of the boundary conditions, in Ref. 65. In particular, for the uniform—either Dirichlet or Neumann—boundary conditions, the coefficients p_n are symmetric with respect to the sign change: $p_n^{(+)} = p_n^{(-)}$.^{58,61,63–65} However, for the DN and ND configurations due to the broken transverse symmetry, this equation does not hold.⁶⁵ Here, we mention also that the functions $\chi_{p_n}(y)$ are expressed through the combination of the Weber parabolic cylinder functions $U(c, \zeta)$,^{66,67} and for every permutation of the boundary requirements,^{58,61,63–65} they obey the same orthonormalization condition,

$$\int_{-1/2}^{1/2} (p_n + p_{n'} - 2By)\chi_{p_n}(y)\chi_{p_{n'}}(y)dy = \delta_{nn'} \quad (9)$$

($\delta_{nn'}$ is a Kronecker symbol), which can be easily derived from the general properties of the Sturm–Liouville analysis.⁶⁸ For the uniform boundary requirements, a countable infinite set of wave vectors p_n contains a finite number of real values, infinitely many purely imaginary values, and—for some magnitudes of B and E —can also include complex numbers.^{58,61,63–65} For the DN and ND boundary conditions, in addition to the finite number of real p_n , a solution of Eq. (3) contains an infinite number of complex states.⁶⁵

In the same way, a solution after the bend reads

$$\Psi(x_1, y_1) = \sum_{n=1}^{\infty} F_n \chi_{p_n^{(+)}(y_1)} e^{ip_n^{(+)} x_1}. \quad (10)$$

Again, the terms in Eq. (10) with real p_n describe the waves propagating away from the scatterer, while the terms with purely imaginary momenta are the states trapped by the bend. Equation (10) is written in the Landau gauge $\mathbf{A} = (-y_1 B, 0)$ for the right arm.

Expression (5) for the current (for ferromagnets) or supercurrent (for superconductors) density in our dimensionless units reads

$$\mathbf{j} = -\text{Im}[\Psi^*(\mathbf{r}) \nabla \Psi(\mathbf{r})] - \mathbf{A} \Psi^*(\mathbf{r}) \Psi(\mathbf{r}). \quad (11)$$

Substituting into it Eqs. (8) and (10), integrating \mathbf{j} over the strip width, and utilizing Eq. (9), one can find the total longitudinal supercurrent flowing in both straight arms. Current conservation gives after the straightforward calculation described above,

$$\sum_{n=1}^{\infty} |C_n|^2 = \sum_{n=1}^{\infty} (|F_n|^2 + |D_n|^2), \quad (12)$$

i.e., the incident flux is equal to the sums of the transmitted and reflected supercurrents.

In a standard manner, one can define scattering \mathbf{S} and reflection \mathbf{R} matrices of the structure that link, respectively, the amplitudes of the transmitted or reflected waves in each subband with those of the incident flux:

$$\mathbf{F} = \mathbf{S}\mathbf{C}, \quad (13a)$$

$$\mathbf{D} = \mathbf{R}\mathbf{C}, \quad (13b)$$

where the amplitudes C_n , F_n , and D_n from Eqs. (8) and (10) form infinite column vectors \mathbf{C} , \mathbf{F} , and \mathbf{D} , respectively. For the ferromagnetic arrangement, scattering matrix \mathbf{S} defines the conductance G of the strip,⁶⁹

$$G(E) = \sum_{nn'} S_{nn'}^* S_{nn'}, \quad (14)$$

with the summation running over all open channels. In the case of superconductors, the conductance is infinite; however, still, matrices \mathbf{S} and \mathbf{R} are relevant; in particular, the term $|S_{11}|^2$ defines a transmission through the bend in the fundamental propagating mode. We note here that the unitarity of the scattering process is mathematically expressed as

$$\mathbf{S}^\dagger \mathbf{S} + \mathbf{R}^\dagger \mathbf{R} = \mathbf{I}, \quad (15)$$

where \mathbf{I} is the unitary matrix. Some other properties of \mathbf{S} and \mathbf{R} are discussed in Ref. 65.

In the curved section, for the up-turn bend, in the polar system of coordinates (ρ, ϕ) with its origin at the center of the bend and polar axis coinciding with the vertical junction between the straight and curved parts, in the symmetric gauge for the vector potential,

$$\mathbf{A} = \left(0, \frac{1}{2}B\rho\right), \quad (16)$$

the radial and angular variables are separated,

$$\Psi(\rho, \phi) = \sum_{n=1}^{\infty} Q_n R_{v_n}(\rho) e^{iv_n \phi}, \quad (17)$$

and the radial wave function $R_{v_n}(\rho)$ satisfies the following equation:

$$\left[\frac{d^2}{d\rho^2} R_{v_n}(\rho) + \frac{1}{\rho} \frac{d}{d\rho} R_{v_n}(\rho) + \pi^2 E R_{v_n}(\rho) \right] - \left(\frac{v_n}{\rho} + \frac{1}{2}B\rho \right)^2 R_{v_n}(\rho) = 0. \quad (18)$$

Similar to the straight arms, our choice of the vector potential [Eq. (16)] leads at $\rho = \rho_0$ and $\rho = \rho_0 + 1$ either to the Dirichlet or Neumann requirement for the radial wave function. As a representative example, below we write an explicit analytical form of the radial function for the DN case,

$$\begin{aligned} R_{v_n}(\rho) = & \gamma_{v_n} \exp\left(-\frac{1}{4}B\rho^2\right) \left(\frac{1}{2}B\rho^2\right)^{v_n/2} \\ & \times \left[M\left(\frac{1}{2} + v_n - \frac{\pi^2 E}{2B}, v_n + 1, \frac{1}{2}B\rho_0^2\right) \right. \\ & \times U\left(\frac{1}{2} + v_n - \frac{\pi^2 E}{2B}, v_n + 1, \frac{1}{2}B\rho^2\right) \\ & \left. - U\left(\frac{1}{2} + v_n - \frac{\pi^2 E}{2B}, v_n + 1, \frac{1}{2}B\rho_0^2\right) \right] \end{aligned}$$

$$\times M\left(\frac{1}{2} + \nu_n - \frac{\pi^2 E}{2B}, \nu_n + 1, \frac{1}{2}B\rho^2\right). \quad (19)$$

Here, $M(a, b, x)$ and $U(a, b, x)$ are Kummer confluent hypergeometric functions⁶⁷ and γ_{ν_n} is determined from the normalization condition of the following form:

$$\int_{\rho_0}^{\rho_0+1} \left(\frac{\nu_n + \nu_{n'}}{\rho} + B\rho \right) R_{\nu_n}(\rho) R_{\nu_{n'}}(\rho) d\rho = \delta_{nn'}. \quad (20)$$

This orthonormalization condition is identical for all other types of the boundary requirements, which again can be derived from the Sturm–Liouville analysis.⁶⁸ In order to distinguish the Weber function $U(a, x)$ from the confluent hypergeometric function $U(a, b, x)$, we write each of them with all their variables.

The boundary condition $\Psi(\rho_0, \phi) = 0$ is automatically satisfied by Eq. (19). Imposing the second condition $\partial\Psi(\rho, \phi) \partial\rho|_{\rho=\rho_0+1} = 0$, one gets the transcendental equation for determining the allowed values of ν_n ; for example, for the DN case, it reads

$$\begin{aligned} & M(a + \nu_n, \nu_n + 1, z_1) \left[\frac{1}{2}(\nu_n - z_2)U(a + \nu_n, \nu_n + 1, z_2) \right. \\ & \quad \left. + z_2 U'(a + \nu_n, \nu_n + 1, z_2) \right] - U(a + \nu_n, \nu_n + 1, z_1) \\ & \quad \times \left[\frac{1}{2}(\nu_n - z_2)M(a + \nu_n, \nu_n + 1, z_2) \right. \\ & \quad \left. + z_2 M'(a + \nu_n, \nu_n + 1, z_2) \right] = 0. \end{aligned} \quad (21)$$

Here, $a = 1/2 - (\pi^2/2)(E/B)$, $z_1 = \rho_0^2/2$, $z_2 = (\rho_0 + 1)^2/2$, and a prime denotes a derivative of the function with respect to its last argument. Equation (21) determines the values of ν_n for the fixed energies E , fields B , and radius ρ_0 . Similar equations can be easily written for the other types of the boundary conditions; for example, for the ND case, one needs to interchange subscripts “1” and “2” at the variable z . All other properties of the above equations, in particular, their asymptotics in the vanishing fields, can be directly analyzed in the same way, as for the DD case.⁵⁸

Contrary to the systems with circular symmetry,^{28,31,38,43,70–76} in our case, the coefficients ν_n are not real integers. An analysis shows that, similar to the DD configuration,⁵⁸ for each fixed energy E , a complete set of solutions of Eq. (21) consists of zero or several real radial wave vectors and a countable infinite number of complex values that are arranged in pairs in such a way that each ν_n has its complex conjugate ν_n^* also satisfying Eq. (21) with the corresponding oscillatory damped wave function having the same real and opposite imaginary parts. Figure 3 provides a comparative analysis of the angular wave vectors ν_n for all four possible cases of the boundary conditions. For complex wave vectors, only their positive imaginary parts are depicted. A strong qualitative similarity for all four cases is seen; namely, for each complex ν_n , the magnitude of its imaginary part decreases with growing energy, and at some value—which is boundary-condition specific—it turns to

zero. At this point, the real part of the wave vector splits into two, which develop into the opposite directions with further growth of E . Discussion of all other properties of the constants ν_n and corresponding functions $R_{\nu_n}(\rho)$ in a straightforward way may be borrowed from the corresponding parts of the description of the DD case;⁵⁸ in particular, solutions of two equations, $\nu_n(E) = 0$ and

$$\frac{\partial E}{\partial \text{Im}(\nu_n)} \Big|_{\partial^2 E / \partial [\text{Im}(\nu_n)]^2 \neq 0} = 0, \quad (22)$$

are identical for the vanishing fields only with their difference growing with B . It is important to note that for the DN case, similar to the DD strip, solutions of Eq. (22) are always smaller than their corresponding cutoff energies for the straight arms.⁶⁵ This is a necessary condition for the existence of the bound states with energies below the fundamental propagation threshold of the straight waveguide.^{50,53,58}

After having found the solutions in each part of the waveguide, one needs to match them at the junctions. However, before doing that, these solutions should be brought to the form where they are expressed in the same gauge. Recall that the order parameter $\Psi(\mathbf{r})$ in the straight arms was derived with the corresponding local Landau gauges described above and in the curved section a symmetric gauge [Eq. (16)] has been implemented. Basic principles of quantum mechanics²⁵ require that the change in the vector potential $\mathbf{A} \rightarrow \mathbf{A} + \nabla f$ should be accompanied by the corresponding transformation of the wave function, $\Psi(\mathbf{r}) \rightarrow \Psi(\mathbf{r})e^{-if(\mathbf{r})}$, where $f(\mathbf{r})$ is an arbitrary function of space. By applying this rule to our situation and choosing as a global gauge the symmetric one, we need to multiply the right-hand side of Eq. (8) by the factor $\exp[-iBx(y + \rho_0 + 1/2)/2]$. The same exponent (with the obvious change $x \rightarrow x_1$, $y \rightarrow y_1$) appears in the corresponding part of Eq. (10). After that, a matching is done for the up-turn bend with the use of the relations between different systems of coordinates (x, y) , (ρ, ϕ) , and (x_1, y_1) ,

$$(x = 0, y) \Leftrightarrow \left(-y + \rho_0 + \frac{1}{2}, \phi = 0 \right), \quad (23a)$$

$$(x_1 = 0, y_1) \Leftrightarrow \left(-y_1 + \rho_0 + \frac{1}{2}, \phi = \phi_0 \right), \quad (23b)$$

$$\frac{\partial}{\partial x} \Big|_{x=0} \Leftrightarrow \frac{1}{-y + \rho_0 + \frac{1}{2}} \frac{\partial}{\partial \phi} \Big|_{\phi=0}, \quad (23c)$$

$$\frac{\partial}{\partial x_1} \Big|_{x_1=0} \Leftrightarrow \frac{1}{-y_1 + \rho_0 + \frac{1}{2}} \frac{\partial}{\partial \phi} \Big|_{\phi=\phi_0}. \quad (23d)$$

As a result of matching, one can express coefficients D_n and F_n via C_n according to Eqs. (13a) and (13b).

The procedure of finding the scattering and reflection matrices for the down-turn bend is very similar to the one of the up-turn case described above. Due to the fixed direction of the particle motion in the uniform magnetic field, now we need to choose the polar axis coinciding with the other junction between the curved and straight sections and the azimuthal angle ϕ growing again in the counterclockwise direc-

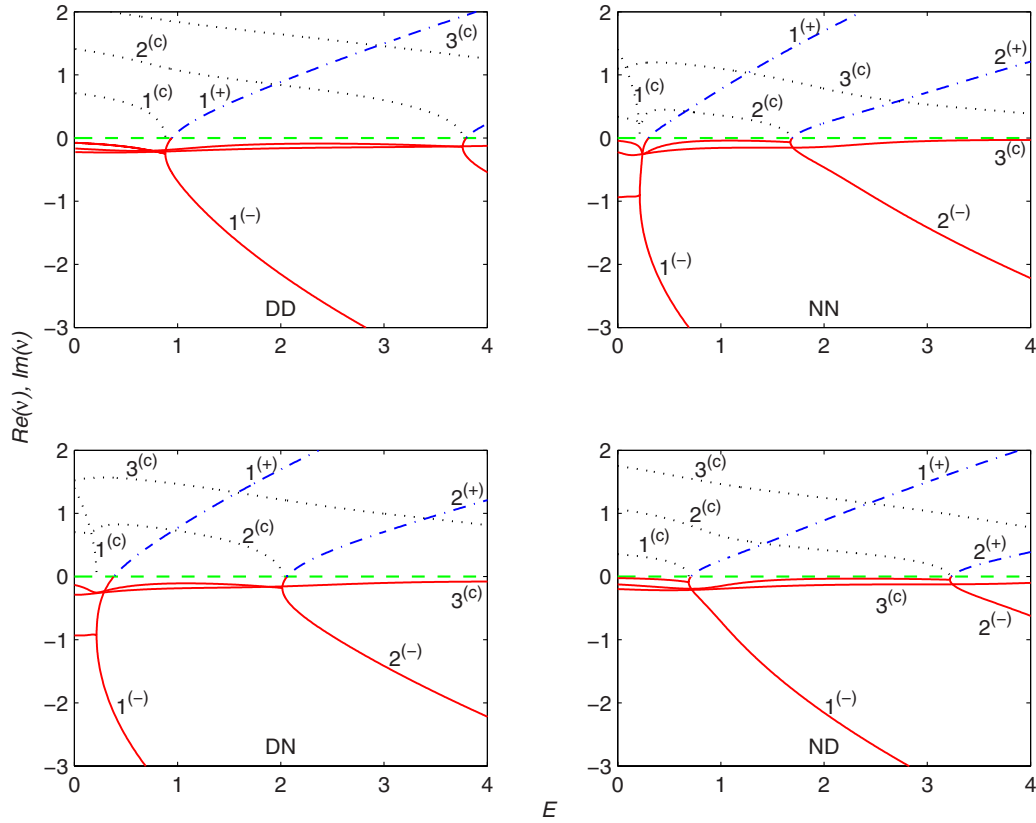


FIG. 3. (Color online) Propagation constants ν_n of the continuously curved waveguide as a function of the energy E for $\rho_0=0.01$ and $B=5$ and four possible types of boundary conditions. States with positive (negative) ν_n are plotted by the dash-dotted (solid) lines and denoted by the corresponding superscript near the level numbers. Real parts of the states with complex propagation constants are also shown by the solid lines and denoted by the superscript (c). Positive imaginary parts of the complex ν_n are plotted by the dotted curves. The dashed lines denote zero value of the angular constant. Two characters in each panel show the corresponding type of the boundary conditions.

tion, as shown by the curved arrow in Fig. 2(b). Accordingly, Eqs. (23a)–(23d) will also be changed,

$$(x_1=0, y_1) \Leftrightarrow \left(y_1 + \rho_0 + \frac{1}{2}, \phi=0 \right), \quad (24a)$$

$$(x=0, y) \Leftrightarrow \left(y + \rho_0 + \frac{1}{2}, \phi = \phi_0 \right), \quad (24b)$$

$$\left. \frac{\partial}{\partial x_1} \right|_{x_1=0} \Leftrightarrow - \frac{1}{y_1 + \rho_0 + \frac{1}{2}} \left. \frac{\partial}{\partial \phi} \right|_{\phi=0}, \quad (24c)$$

$$\left. \frac{\partial}{\partial x} \right|_{x=0} \Leftrightarrow - \frac{1}{y + \rho_0 + \frac{1}{2}} \left. \frac{\partial}{\partial \phi} \right|_{\phi=\phi_0}. \quad (24d)$$

In all other aspects, the procedure of deriving the scattering \mathbf{S} and reflection \mathbf{R} matrices remains the same, as described above. Since explicit expressions for \mathbf{S} and \mathbf{R} are very similar to the ones of the DD case,⁵⁸ we do not write them here.

When one considers bound states lying below the fundamental propagation threshold of the straight DN arm, it is necessary to set all coefficients C_n in Eq. (8) equal to zero, $C_n \equiv 0$. The procedure of matching is completely similar to the one used for the scattering case and leads then to the infinite linear algebraic system. Requirement of the vanish-

ing of its determinant defines energies of the bound levels and, according to Eq. (4), temperatures T at which a nucleation of superconductivity takes place. An infinite set of eigenvectors corresponding to the eigenenergies defines coefficients D_n , F_n and Q_n . In other words, one can fully construct the order parameter Ψ in the magnetic field.

III. RESULTS AND DISCUSSION

Here, we present results of the theory developed in Sec. II with their detailed analysis. Since, as we pointed out earlier, for the DN superconducting strip the critical temperature is higher than for its straight counterpart, the main attention will be paid just to this configuration of the boundary conditions. However, before doing this, we want to return to the applicability of our model to the magnetic materials. Namely, the Neumann boundary condition at the interface naturally arises in the GL description of superconducting samples. On the other hand, for the magnetic multilayers, it needs some additional justification provided below. As we have shown in Sec. I for the field-free straight waveguide with the potential profile depicted in Fig. 1(a), mixed boundary conditions can be achieved for $V_0=(1/s^2-1)/4$ and quite small s . In turn, in the curved section with an outer deeper well, the propagation thresholds W_n are determined from the following equation:

$$\begin{aligned}
& \sqrt{1 + \frac{V_0}{W_n}} \{Y_0[\pi\sqrt{W_n + V_0}(\rho_0 + 1 + s)]J_1(\pi\sqrt{W_n + V_0}(\rho_0 + 1)) - J_0[\pi\sqrt{W_n + V_0}(\rho_0 + 1 + s)]Y_1[\pi\sqrt{W_n + V_0}(\rho_0 + 1)]\} \\
& \times \{Y_0(\pi\sqrt{W_n\rho_0})J_0[\pi\sqrt{W_n}(\rho_0 + 1)] - J_0(\pi\sqrt{W_n\rho_0})Y_0[\pi\sqrt{W_n}(\rho_0 + 1)]\} - \{Y_0[\pi\sqrt{W_n + V_0}(\rho_0 + 1 + s)]J_0[\pi\sqrt{W_n + V_0}(\rho_0 + 1)] \\
& - J_0[\pi\sqrt{W_n + V_0}(\rho_0 + 1 + s)]Y_0[\pi\sqrt{W_n + V_0}(\rho_0 + 1)]\} \{Y_0(\pi\sqrt{W_n\rho_0})J_1[\pi\sqrt{W_n}(\rho_0 + 1)] - J_0(\pi\sqrt{W_n\rho_0})Y_1[\pi\sqrt{W_n}(\rho_0 + 1)]\} = 0,
\end{aligned} \tag{25}$$

where $J_\nu(x)$ and $Y_\nu(x)$ are the ν th order Bessel functions.⁶⁷ For $V_0=(1/s^2-1)/4$, the limit of $s \rightarrow 0$ transforms Eq. (25) to

$$\begin{aligned}
& \{Y_0(\pi\sqrt{W_n\rho_0})J_1[\pi\sqrt{W_n}(\rho_0 + 1)] - J_0(\pi\sqrt{W_n\rho_0})Y_1[\pi\sqrt{W_n}(\rho_0 + 1)]\} \\
& = \frac{1}{2\pi(\rho_0 + 1)\sqrt{W_n}} \{Y_0(\pi\sqrt{W_n\rho_0})J_0[\pi\sqrt{W_n}(\rho_0 + 1)] - J_0(\pi\sqrt{W_n\rho_0})Y_0[\pi\sqrt{W_n}(\rho_0 + 1)]\},
\end{aligned} \tag{26}$$

while for the Dirichlet–Neumann configuration, the right-hand side of this equation is identically zero.⁵³ When utilizing properties of the Bessel functions,⁶⁷ it is elementary to show that in the limiting case of $\rho_0 \rightarrow \infty$, Eq. (26) reproduces straight Dirichlet–Neumann thresholds from Eq. (2), as would be expected. Note that for the zero left-hand side, one gets the equation for the determination of the bend propagation thresholds for the DD strip.⁵¹ Thus, contrary to the straight arms, where the limiting procedure of $s \rightarrow 0$ leads to the DN configuration, in the bend, one arrives to the more complicated situation. Semiclassically, this difference that decreases with increasing ρ_0 is explained by the centrifugal forces acting in the curved section and being absent in the straight arms. Figure 4 depicts radial wave functions for the fundamental ($n=0$) and first propagating ($n=1$) bend thresholds and several s with $\rho_0=0.1$. It is seen that contrary to the straight waveguide, even for the flat potential profile, the wave function is *not* symmetric with respect to the middle of the bend (dotted curves in Fig. 4). Accordingly, decreasing width s , in general, does not lead to the vanishing derivative of the wave function at $\rho=\rho_0+1$. A comparative analysis of the two cases of Eq. (26) (with zero and nonzero right-hand sides) shows that the threshold energies W_n for the former case are smaller than their counterparts for the latter situation, which physically means that the DN bend binds electron stronger than the limiting case of the potential from Fig. 1(a). As an example, we show in Fig. 5(b) bound-state energies of the curved waveguide with DN boundaries⁵³ and of the duct with stepped potential for $s=0.01$ and different V_0 . As expected, for $V_0=(1/s^2-1)/4$, at $\phi_0=0$, the bound state emerges with energy $E=1/4$, as is the case for the DN quantum wire too.⁵³ Increasing bend angle ϕ_0 in both cases causes the bound-state energies to decrease with the slope of the curve for the DN channel being steeper. As stressed above, smaller bound-state energies for the DN case are due to the stronger electron confinement in the bend. However, as shown in Fig. 5(b), any desired bound-state energy of the DN waveguide can be achieved in the model of the channel with the stepped potential by tiny changes in V_0 ; for example, to match the DN energy at $\phi_0=120^\circ$, one needs to increase the depth of the outer well by only $\sim 0.2\%$. Thus, here the proposed model of the stepped potential profile can serve as a

very good first approximation for the mixed boundary conditions in the magnetic multilayers. We also show in Fig. 5(a) bound-state energies of the stepped potential for different widths s and $V_0=(1/s^2-1)/4$. It is seen that smaller s causes the energies to decrease faster with their difference increasing with the bend angle ϕ_0 .

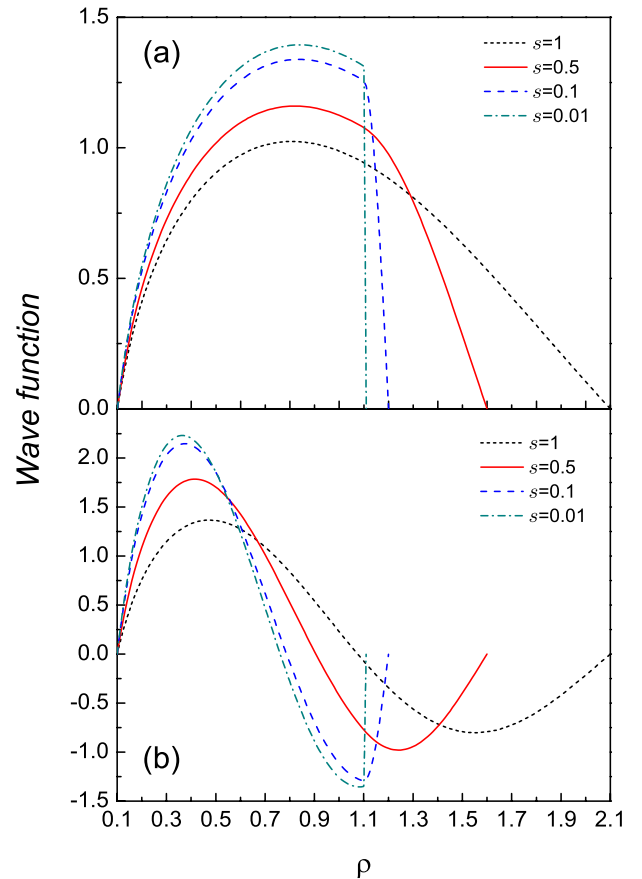


FIG. 4. (Color online) (a) Radial wave functions of the fundamental bend propagation threshold ($n=0$) for the gap $V_0=(1/s^2-1)/4$ and several lengths s . (b) The same as in panel (a), but for the first excited propagation threshold ($n=1$). The bend radius for both cases is $\rho_0=0.1$.

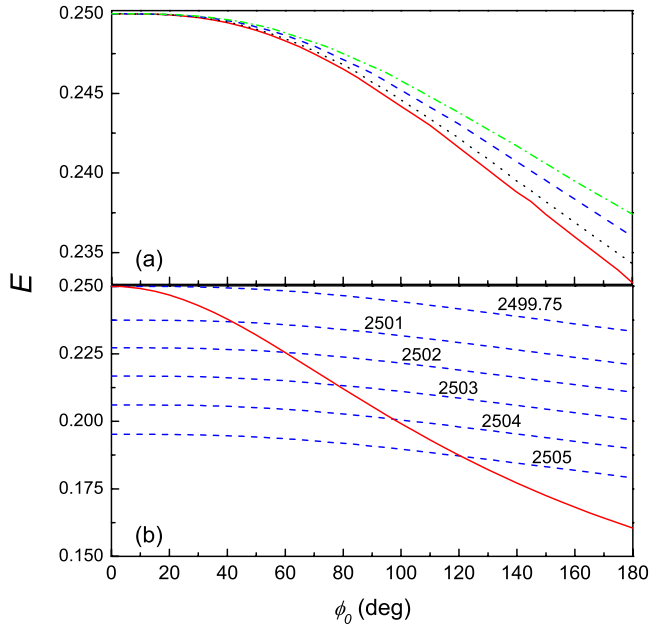


FIG. 5. (Color online) (a) Bound-state energies of the curved wire with stepped transverse potential profile for the gap $V_0 = (1/s^2 - 1)/4$ and several lengths s as a function of the bend angle ϕ_0 : the solid curve is for $s=0.001$, the dotted curve is for $s=0.1$, the dashed curve is for $s=0.3$, and dash-dotted line is for $s=0.5$. (b) Bound-state energies of the curved DN waveguide (solid line) and of the wire with the stepped transverse potential with $s=0.01$ and several depths V_0 (dashed curves). The numbers above the dashed curves denote corresponding depth V_0 . The upper curve is for $V_0 = (1/s^2 - 1)/4$. The bend radius for both panels is $\rho_0=0.1$.

Having learned about the applicability of the model with the mixed boundary conditions, we return to the analysis of the magnetic field influence on the bent waveguide. We start from the localized modes. Our calculations show that their energies, similar to the DD case,⁵⁸ are independent of the field orientation. Accordingly, below, we will discuss the case of positive B only. Figure 6 shows bound-state energies of the DN up-turn film for several ρ_0 and ϕ_0 . Recalling Eq. (4), one can say that Fig. 6 shows $B-T_c$ phase boundary for the superconducting strip. For comparison, the boundary for the straight DN duct is also shown. It was obtained in the manner analogous to the NN channel;⁴⁰ namely, first, a lowest solution E of the corresponding transcendental equation,

$$U \left[\frac{\pi^2 E}{2B}, -i(2B)^{1/2} \left(\frac{1}{2} - \frac{p}{B} \right) \right] U' \left[\frac{\pi^2 E}{2B}, -i(2B)^{1/2} \left(\frac{1}{2} + \frac{p}{B} \right) \right] + U \left[\frac{\pi^2 E}{2B}, i(2B)^{1/2} \left(\frac{1}{2} - \frac{p}{B} \right) \right] \times U' \left[\frac{\pi^2 E}{2B}, i(2B)^{1/2} \left(\frac{1}{2} + \frac{p}{B} \right) \right] = 0, \quad (27)$$

was calculated for the fixed arbitrary momentum p and, next, this solution was minimized with respect to p . It is seen from Fig. 6 that energies monotonically increase with the field, which, quite naturally, means decreasing critical temperature T of the superconducting film. Remarkably, for all bend radii

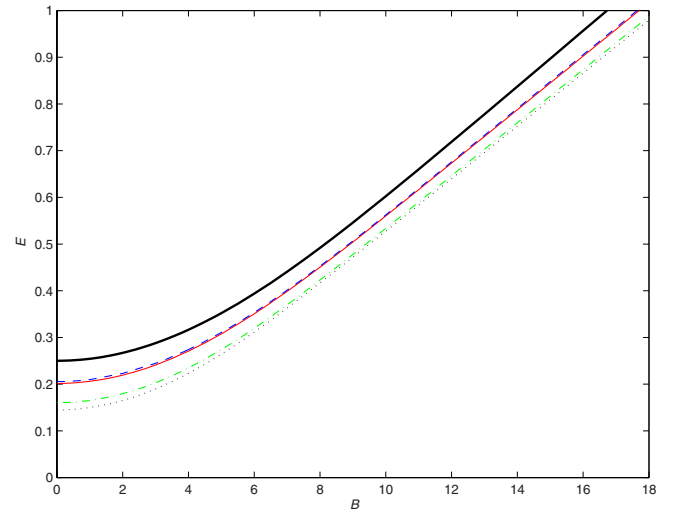


FIG. 6. (Color online) Bound-state energies E as a function of the field B for $\rho_0=0.001$ and $\phi_0=90^\circ$ (thin solid line), $\rho_0=0.001$ and $\phi_0=180^\circ$ (dotted line), $\rho_0=0.1$ and $\phi_0=90^\circ$ (dashed line), and $\rho_0=0.1$ and $\phi_0=180^\circ$ (dashed-dotted line). The thick solid line shows the fundamental propagation threshold of the corresponding straight film [least solution of Eq. (27)].

and angles, the critical temperature for the curved film remains higher than for its straight counterpart. In other words, bend-induced enhancement of the superconductivity in zero fields⁵³ persists for nonzero B . Similar to the DD case,⁵⁸ bound-state wave function in the straight arms contains components χ_{p_n} with only complex wave vectors p_n while in the bend, in addition to the infinite set of complex ν_n , there are two waves with real coefficients ν_n freely propagating in the curved section. We also note that contrary to the DD curved channel,⁵⁸ the energies for the DN case grow slower with the field, and at high B they do not approach Landau levels staying well below them. This, of course, is due to the influence of the Neumann surface.

Figure 7 shows the order parameter $\Psi(\mathbf{r})$ of the right angle bend with $\rho_0=0.001$ for several nonzero magnetic fields. The corresponding plot for $B=0$ is depicted in Fig. 4 of Ref. 53. Increasing magnetic intensity pushes Cooper pairs closer to the boundary with the Neumann requirement where the nucleation of superconductivity takes place. It also leads to the larger longitudinal extent of Ψ in the straight arms, which means that superconductivity for the higher B nucleates not only in and around the bend, as it was the case for zero and small fields, but is disseminated further and further along the Neumann edge. For all magnetic fields, the order parameter remains symmetric with respect to the plane $\phi = \phi_0/2$.

Next, we consider transmission properties of the bend as a function of energy E for different B . Due to the size quantization imposed by the finite strip width, a transport in the film takes place in subbands that, for zero magnetic field, have their thresholds at $E_n^{DN} = (n + 1/2)^2$, $n=0, 1, \dots$. Their evolution for nonzero field is discussed in Ref. 65. As follows from Eq. (4), energy change is equivalent to the varying temperature T . For example, for typical experimental parameters $\xi(0)=120$ nm and $d=1$ μm ,³⁸ one has

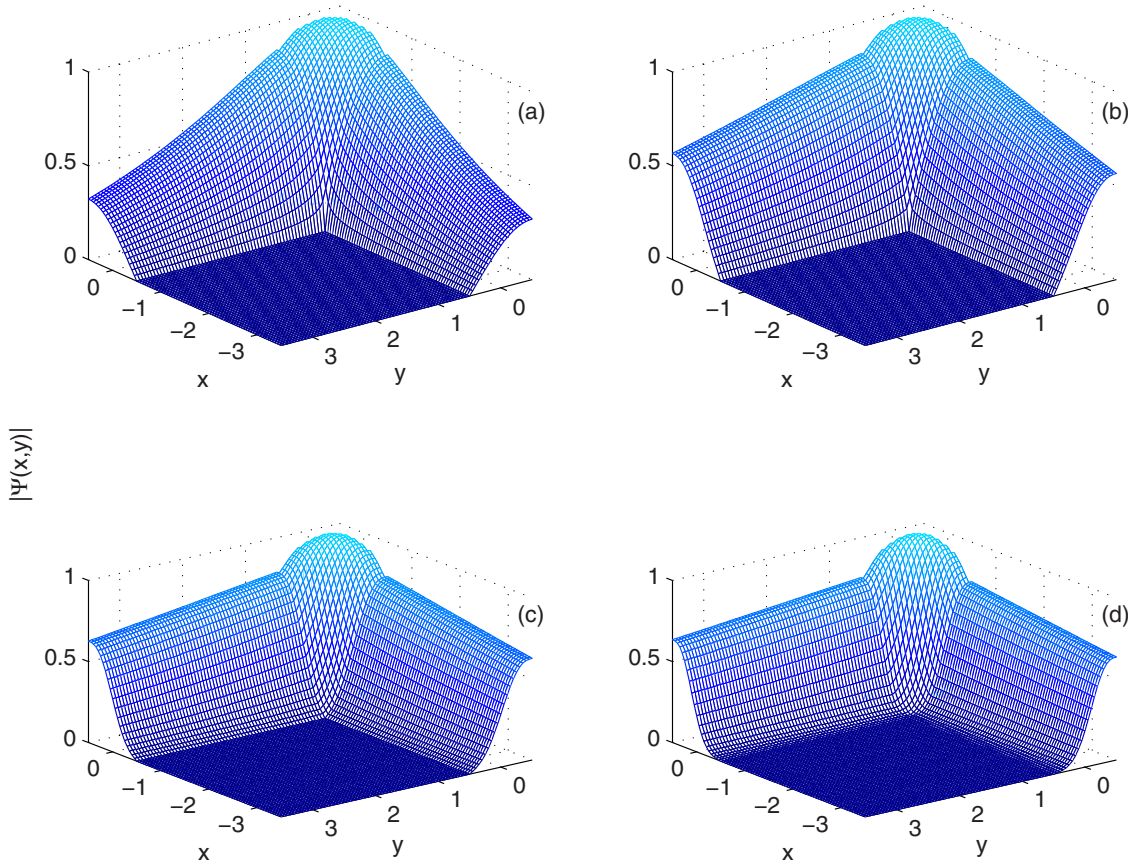


FIG. 7. (Color online) Order parameter $|\Psi(x,y)|$ (normalized to its maximum) of the bound state for $\rho_0=0.001$ and the right angle for (a) $B=2$, (b) $B=5$, (c) $B=10$, and (d) $B=15$.

$$\frac{T}{T_c} = 1 - 0.14E. \tag{28}$$

Accordingly, the fundamental propagation threshold for zero magnetic field $E=1/4$ is equivalent to $T_1=0.964T_c$, and the upper boundary of the first propagating mode $E=9/4$ to $T_2=0.680T_c$. Note that due to the substitution of one of the Neumann edges by the Dirichlet one, no supercurrent flows for the temperatures in the range $T_1 \leq T \leq T_c$. This is in a sharp contrast to the NN case when the thresholds are given by $E_n^{NN}=n^2$, $n=0,1,2,\dots$, and, accordingly, a continuous spectrum starts at $E=0$. Below, in order to eliminate the interference between the modes that might obscure the most characteristic features of discussed phenomena, we will confine our consideration to the fundamental mode only when the term $|S_{11}|^2$ is relevant. Our results show that in this case, there is no difference in the transmission between up- and down-turn bends. Thus, in the following, we will talk about the magnitude of the magnetic field B only, without reference to the up- or down-turn configuration.

Figure 8 shows the transmission through the bend with $\rho_0=0.001$ and $\phi_0=180^\circ$ for several magnetic fields. For the field-free case, there are one or several Breit–Wigner-type resonances near the fundamental propagation threshold and a steep antiresonance with zero transmission slightly below the upper boundary.⁵³ This antiresonance is explained by mixing by the bend of the longitudinal and transverse motions in the

waveguide and the interference of the discrete level split off by the bend from the higher lying subband, with the continuum states of the fundamental mode. As a result, the an-

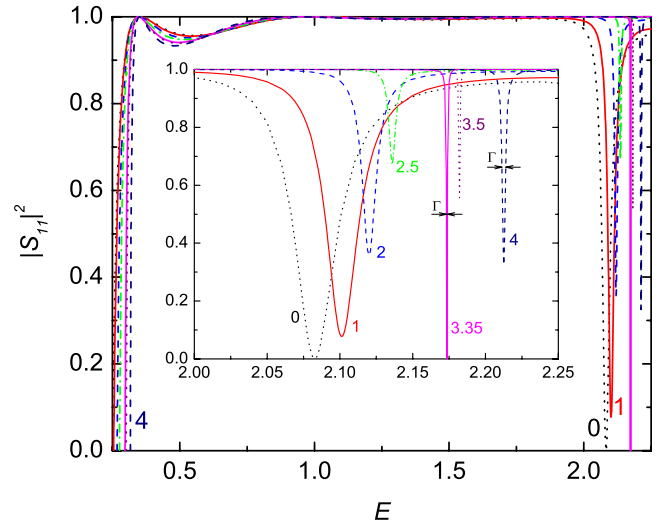


FIG. 8. (Color online) Transmission $|S_{11}|^2$ as a function of the energy E for the bend with $\rho_0=0.001$ and $\phi_0=180^\circ$ for several values of the magnetic field B . The inset shows the enlarged view near the mode upper threshold. The numbers near the curves denote corresponding intensity B . The arrows show half widths Γ for $B=3.35$ and $B=4$.

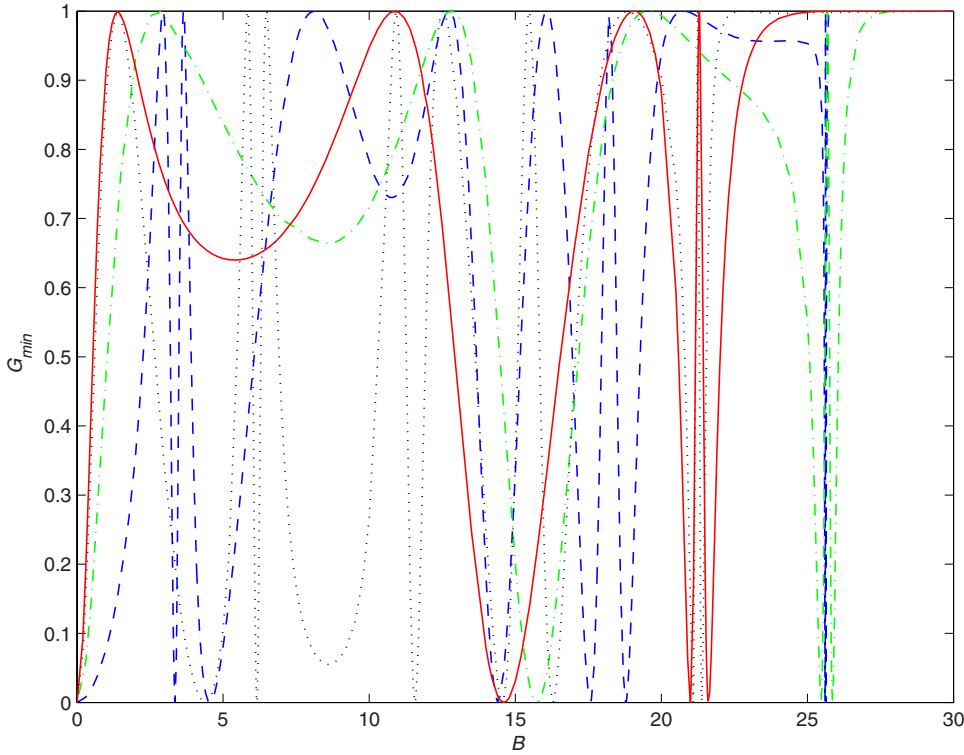


FIG. 9. (Color online) Transmission G_{\min} corresponding to the minimum on $|S_{11}|^2-E$ curve as a function of the field B for $\rho_0=0.1$ and $\phi_0=90^\circ$ (solid curve), $\rho_0=0.1$ and $\phi_0=180^\circ$ (dotted curve), $\rho_0=0.001$ and $\phi_0=90^\circ$ (dashed-dotted curve), and $\rho_0=0.001$ and $\phi_0=180^\circ$ (dashed curve).

tiressonance is formed with the energy of the zero minimum E_{\min} and the half width Γ , which depend on the parameters of the bend.

Applied magnetic field drastically modifies transmission dependence on the energy E with main influence being exerted on the zero antiresonance with only slight changes in the resonances near the fundamental propagation threshold. As shown in Fig. 8, the energy E_{\min} at which the minimum is achieved increases with the field. Its B dependence is similar to the bound-state energies described above. The minimum conductance G_{\min} generally ceases to be zero for nonvanishing magnetic fields. For example, for the parameters from Fig. 8, it grows with small fields, reaching unity maximum at $B=2.95$, which means that at this point, the resonance is completely dissolved. After that, the value $|S_{11}|^2$ decreases with the zero minimum being again achieved at $B=3.35$, and the situation is repeated a few more times. Thus, contrary to the field-free case,⁵³ for the complete description of the resonance, one needs to use not only the energy E_{\min} and the half width Γ which form the complex energy of the quasibound state,

$$E_{qb} = E_{\min} - \frac{i\Gamma}{2}, \quad (29)$$

but also the minimum value of the conductance in the resonance G_{\min} . Accordingly, the definition of the half width Γ that defines the lifetime τ of the corresponding level,

$$\tau = \frac{1}{\Gamma}, \quad (30)$$

should be modified in order to reflect the nonzero minimum of the conductance; namely, as shown in Fig. 8, now it is the

difference between the energies at which the conductance is equal to $G=(1+G_{\min})/2$. It is seen from Fig. 8 that Γ is a nonmonotonic function of the field; in particular, it diverges when the minimum conductance reaches its unity maximum. As we mentioned above, it means a complete dissolution of the quasibound level formed by the bend. Since the $\Gamma-B$ dependence for the DN case is very similar to the pure Dirichlet strip,⁵⁸ it is not shown here.

Transmission in the minimum G_{\min} as a function of the field is shown in Fig. 9. It is seen that minimum transmission oscillates with B , the number of oscillations being larger for the larger bend angle and fixed radius. The maxima of G_{\min} are always equal to unity, while its minima can take vanishing as well as nonzero values. At strong enough magnetic intensities, the minimum transmission approaches unity and retains this magnitude with increasing B . As we mentioned above, this means that the field completely washed out the resonance. On the quantitative note, one sees that, compared to the DD case,⁵⁸ complete dissolution of the quasibound level for the DN case takes place at smaller fields.

To get a deeper insight into the transport properties, it is instructive to investigate currents flowing in the film. We start this discussion from the case of nonvanishing small and moderate fields. Figure 10 shows the current densities \mathbf{j} calculated from Eq. (11) for the up-turn bend with $\rho_0=0.001$ and $\phi_0=180^\circ$ at $B=1$ and several energies E (see corresponding curve in Fig. 8, which reaches its minimum of $G_{\min}=0.077$ at $E_{\min}=2.101$ with a half width $\Gamma=0.026$). It is known⁵³ that current density patterns for the field-free case form the vortices inside and near the bend, which change their chirality as the energy sweeps through E_{\min} . The applied magnetic field changes the vortex behavior. Namely, for the energy far away from E_{\min} , the current flow is perfectly laminar throughout the whole strip with the largest

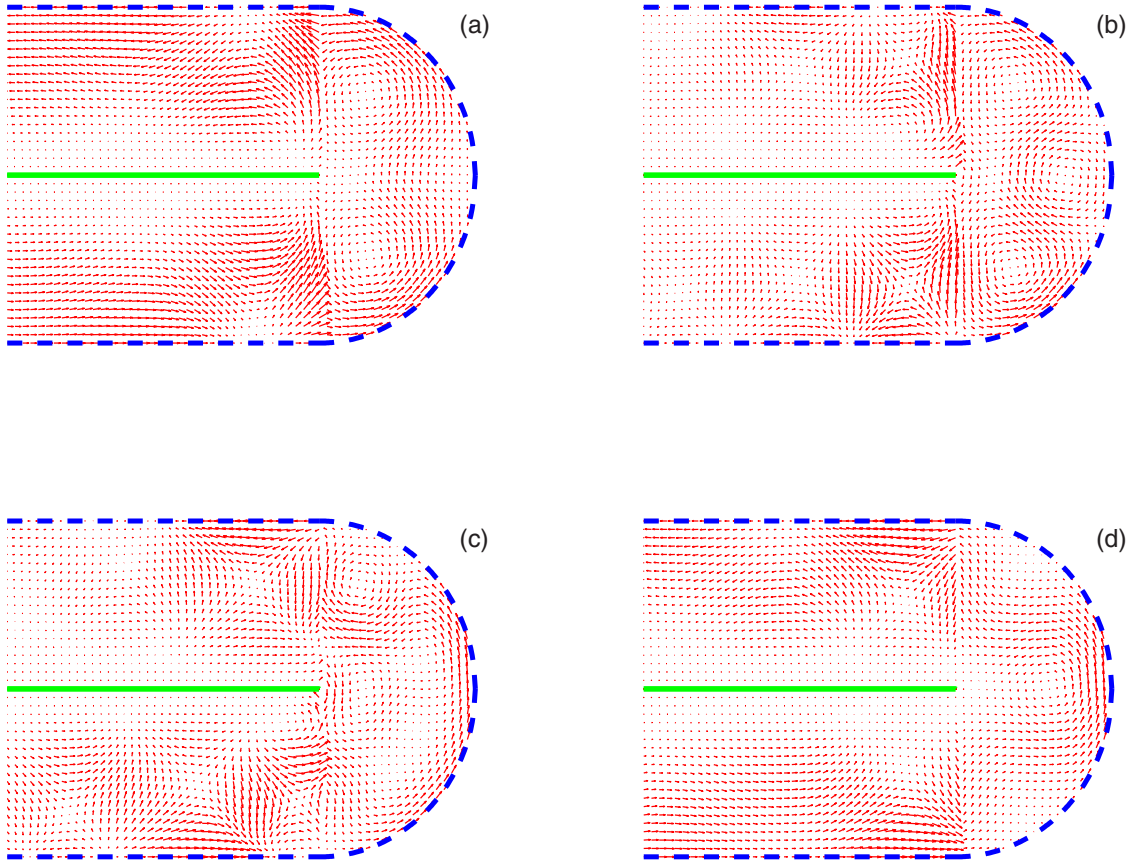


FIG. 10. (Color online) Spatial distribution of the current densities \mathbf{j} of the up-turn strip at magnetic field $B=1$ for $\rho_0=0.001$, $\phi_0=180^\circ$ and several values of the energy E : (a) $E=2.05$ (transmission $|S_{11}|^2=0.957$), (b) $E=2.095$ ($|S_{11}|^2=0.254$), (c) $E=2.11$ ($|S_{11}|^2=0.345$), and (d) $E=2.15$ ($|S_{11}|^2=0.910$). The inner Dirichlet and outer Neumann surfaces of the film are shown by the thick solid and dashed lines, respectively. Since the bend radius is very small, the gap between the two parallel inner walls is not seen in the figure. The larger arrows denote higher currents. For each of the figures, the currents are normalized with respect to their largest value.

longitudinal \mathbf{j} near the Neumann edge. As one comes closer to the resonance, the vortices start to develop inside the curved section. One of the first phases of the formation of the vortices is shown in Fig. 10(a), wherein three well-resolved vortex centers are clearly seen inside the bend with the current density around them acquiring a noticeable transverse component. Contrary to the field-free case,⁵³ in the straight arms instead of the vortices, one sees the formation of the antivortices near the curved section. Far away in the straight arms, the current still has a longitudinal component only. Antivortices develop as a result of the interaction of the surface currents^{77–81} flowing along the opposite edges of the strip. When one comes closer to E_{\min} , whirling motion in the bend becomes more pronounced [Fig. 10(b)] with the antivortices in the straight arms being also clearly observable. Similar to the DD case,⁵⁸ the vorticity of the currents near the junctions with the straight arms is larger than their counterpart in the middle of the curved section. In turn, for the field-free case,⁵³ all the whirlings in the bend have the same strength. Further evolution of the vortices with energy is very similar to the DD case;⁵⁸ namely, with E growing, the vortices move clockwise, retaining their vorticity sign and, upon approaching the junction with the straight part, the lowest vortex is dissolved in it giving birth to the new antivortex [Fig. 10(c)]. Simultaneously, near the upper junction, the

new vortex is formed occupying the place of its predecessor with its vorticity being opposite. Thus, for nonzero magnetic intensities, the change of the vorticity sign is a gradual process, contrary to the field-free case,^{53,82} wherein the whirlings abruptly flip their sign at the energy of the reflection resonance due to the sudden change of the phase of the transmission matrix. As one moves further to the right of the resonance area [Fig. 10(d)], the current gradually restores its laminar character. It is important to emphasize that, similar to the quantum dot embedded symmetrically into the waveguide⁸³ or the two Neumann windows in the straight Dirichlet waveguide,⁶⁵ vortices discussed here are a simple consequence of the geometry-induced interference between the different subbands in the presence of the magnetic field and, as such, they are different from the vortices in the bulk superconductors;^{23,24} in particular, each of them does not carry the flux quantum. It is also worthwhile to note that for all magnetic fields, the current density \mathbf{j} at the Neumann edge has a longitudinal component only, $\mathbf{n}\mathbf{j}=0$, with no flow through the surface, as it should be for the superconductors.^{23,24}

Further growth of the magnetic field leads to the qualitative change of the vortices. Figure 11 shows the current density evolution for the quite strong field $B=15$ for the film with $\rho_0=0.1$ and $\phi_0=180^\circ$ when minimal transmission G_{\min}

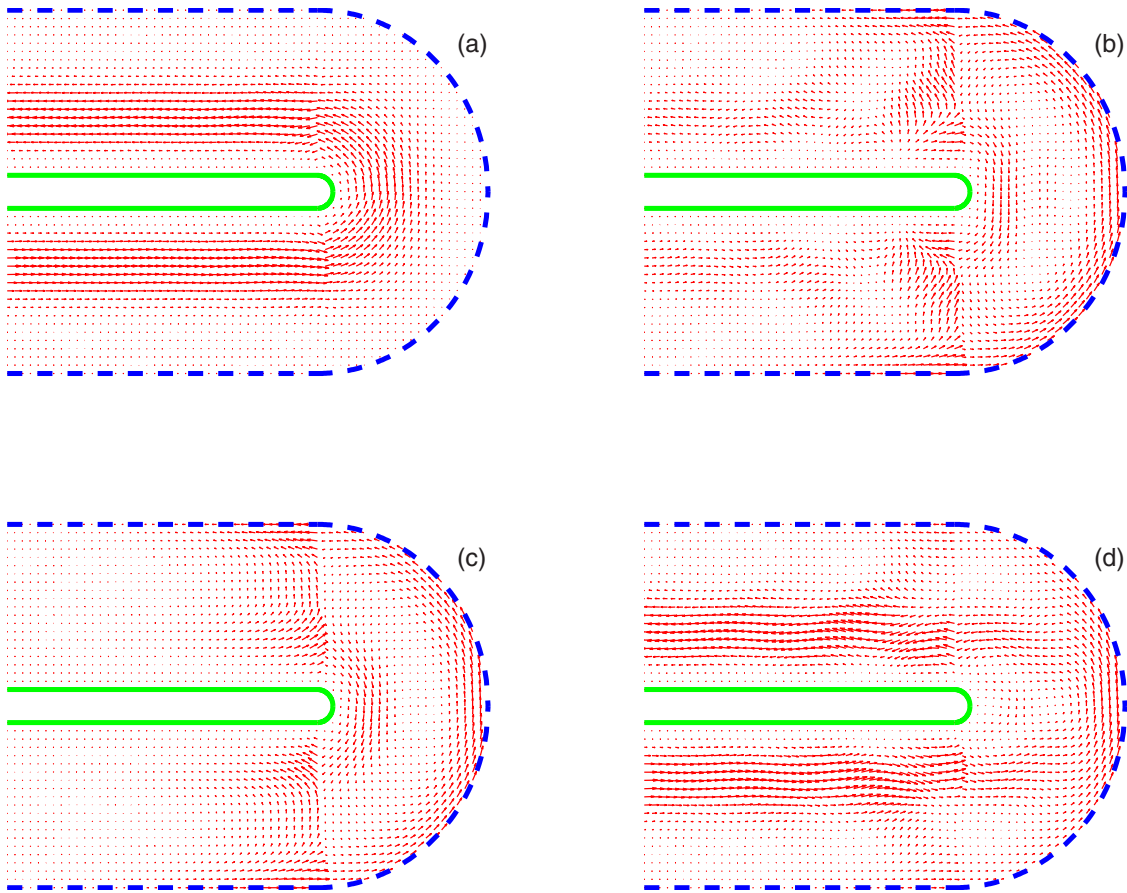


FIG. 11. (Color online) Spatial distribution of the current densities \mathbf{j} of the up-turn film at magnetic field $B=15$ for $\rho_0=0.1$, $\phi_0=180^\circ$ and several values of the energy E : (a) $E=3.94$ ($|S_{11}|^2=1$), (b) $E=3.996$ ($|S_{11}|^2=0.999$), (c) $E=3.998\ 43$ ($|S_{11}|^2=0.352$), and (d) $E=4.005$ ($|S_{11}|^2=1$). For each of the figures, the currents are normalized with respect to their largest value.

$=0.352$ is achieved at $E_{\min}=3.998\ 43$ with a narrow half width $\Gamma=0.000\ 17$. Away from the resonance, the current for the up-turn bend mainly flows in the vicinity of the inner (i.e., Dirichlet) surface, as shown in Fig. 11(a). This is a vivid example of the surface currents in the magnetic fields.^{77–81} In turn, for the down-turn bend, the current in the straight arms, similar to the DD configuration,⁵⁸ will concentrate near the outer surface, i.e., in our case, near the Neumann wall. With energy approaching the resonance, no multiple vortices develop in the bend. Instead, according to Figs. 11(b) and 11(c), only one vortex is observable, which is confined by the curved part and its junctions with the straight arms with current amplitude being 4 orders of magnitude larger than for the flows at the nonresonant energies. The vorticity sign is not changed after passing the minimum E_{\min} . One can say that for strong enough fields, a giant vortex is formed in the bend-induced positive potential. At the energies sufficiently far away from the resonance, the bend-shaped vortex is split into the several irregular patterns shown in Fig. 11(d) with the currents in the straight arms restoring laminar flow near the inner surface. Thus, similar to the DD case, increasing magnetic field reduces number of the vortices. At still higher fields, when the quasibound state is completely dissolved, $G_{\min}=1$, no vortices are formed at all with perfect laminar current flow.

IV. CONCLUDING REMARKS

We have theoretically considered properties of the curved thin film with different boundary conditions in the homogeneous magnetic field. Even though the superconductivity and the magnetism are two opposite, competing, not to say, antagonistic, physical phenomena, we have shown that the proposed model can be equally well applied to these both kinds of strip. As already mentioned, the same model can be used for the study of the processes in graphene,²¹ although it needs relativistic generalization in this case. Our analysis confirmed once again that the pure Dirichlet and the DN bent films have many features in common; previous theoretical research^{52,53} established this fact for the field-free case, and our present calculations proved it for the applied magnetic fields.⁵⁸

Here, the discussed situation of the simultaneous presence of the pure Dirichlet and Neumann requirements is a limiting case of a more general situation when both the wave function Ψ and its derivative enter into the boundary conditions. In terms of Eq. (7), it means the finite nonzero value of the extrapolation length Λ . In mathematics, such a combination is called a Robin boundary condition. Recently, the first theoretical analysis of the field-free curved waveguide with Dirichlet and Robin requirements on the opposite walls was

reported.⁸⁴ Further research will reveal bound-state existence and their dependence on the extrapolation length Λ and the parameters of the bend for both $B=0$ and the nonzero field.

Experimentally, semiconductor technology advanced to such a level that allows researchers to measure miscellaneous spin⁸⁵ and charge⁸⁶ properties of the pure Dirichlet L-shaped structures. In our opinion, the discussed DN curved films could be produced, say, by the appropriate truncation of the superconducting Hall bars⁸⁷ and flanking them with different substrates. Depending on the crystallographic directions, bends with other configurations can also be designed and tested.

Throughout the whole paper, while talking about superconductors, we have used the linearized GL equation. It is known^{22–24} that the full system of GL equations contains in the left-hand side of Eq. (3) the term $\beta|\Psi|^2\Psi$ with the second GL parameter β given by^{23,88} (we return here to the dimensional units)

$$\beta \simeq \frac{1}{N(0)} \left[\frac{\hbar^2}{2m\xi^2(0)} \right]^2 \frac{1}{(k_B T_c)^2}, \quad (31)$$

where $N(0)$ is the density of states at the Fermi energy and k_B is the Planck constant. Expression (31) is valid for the “pure” superconductors. For the “dirty” superconductors (alloys), $\xi^2(0)$ in GL parameters α and β should be substituted by $\xi(0)l$, where l is the mean free path of the material. In the standard treatment of the bound states,^{23,24} the cubic term can be safely neglected since the lowest localized solution corresponds to the nucleation of the superconductivity when the order parameter Ψ representing the density of superconducting electrons is small. As we mentioned in Sec. I, such a theoretical approach is in very good agreement with

experiment.^{36–38} In turn, a solution of the full system of the GL equations for the scattering case presents a formidable challenging problem lying beyond the scope of the present research. Inclusion of the cubic term should modify results presented above. However, we believe that the main features discussed here—such as transmission change with temperature or evolution of the vortices in the magnetic field—will qualitatively survive in such a treatment. First, we note that, as follows from Eq. (31), the relative contribution of the cubic term will be small for the large terms in the denominator of its right-hand side. In particular, for the classical (non-high- T_c) superconductors, the coherence length $\xi(0)$ is rather large compared to the high- T_c materials. Thus, finding optimal combination of T_c and ξ can strongly minimize β . Second, it is known that for small superconducting aluminum disks with radius ρ_0 , the linearized equation correctly captures the essential qualitative features of the magnetization dependence on the magnetic fields⁷⁴ for large enough ρ_0 , and for the smaller radii its solutions quantitatively coincide with the experimental data⁸⁹ even better than those of the full GL system.⁷⁴ Note that experiments⁸⁹ and their theoretical explanations⁷⁴ are carried out down to $T=0.4$ K, lying well below the corresponding $T_c=1.19$ K for aluminum (cf. Ref. 23). In our scattering configuration, such a ratio for $\xi(0)=120$ nm (Ref. 38) and $d=1$ μm corresponds to the dimensionless energy $E \sim 5$ lying in the neighborhood of the upper threshold of the first excited propagating mode. This last argument also shows that the temperature range where the GL theory is applicable is covered by our treatment. Accordingly, the main messages of the present paper concerned to the supercurrents for temperatures below T_c should be present—in more or less modified form—in the more elaborate theories and detected in the experiment.

*Present address: Department of Physics, Jackson State University, Jackson, MS 39217, USA. oleg.olenski@jsums.edu

¹F. J. Himpfel, J. E. Ortega, G. J. Mankey, and R. F. Willis, *Adv. Phys.* **47**, 511 (1998); C. H. Marrows, *ibid.* **54**, 585 (2005); J. I. Martín, J. Nogués, K. Liu, J. L. Vicent, and I. K. Schuller, *J. Magn. Magn. Mater.* **256**, 449 (2003).

²M. B. Salamon, S. Sinha, J. J. Rhyne, J. E. Cunningham, R. W. Erwin, J. Borchers, and C. P. Flynn, *Phys. Rev. Lett.* **56**, 259 (1986); C. F. Majkrzak, J. W. Cable, J. Kwo, M. Hong, D. B. McWhan, Y. Yafet, J. V. Waszczak, and C. Vettier, *ibid.* **56**, 2700 (1986); P. Grünberg, R. Schreiber, Y. Pang, M. B. Brodsky, and H. Sowers, *ibid.* **57**, 2442 (1986).

³P. Bruno, *Phys. Rev. B* **52**, 411 (1995).

⁴B. A. Jones, *IBM J. Res. Dev.* **42**, 25 (1998).

⁵M. D. Stiles, *J. Magn. Magn. Mater.* **200**, 322 (1999).

⁶A. Fert, P. Grünberg, A. Barthélémy, F. Petroff, and W. Zinn, *J. Magn. Magn. Mater.* **140–144**, 1 (1995); P. Grünberg, *Phys. Today* **54**(5), 31 (2001); *J. Phys.: Condens. Matter* **13**, 7691 (2001).

⁷M. N. Baibich, J. M. Broto, A. Fert, F. Nguyen Van Dau, F. Petroff, P. Etienne, G. Creuzet, A. Friederich, and J. Chazelas, *Phys. Rev. Lett.* **61**, 2472 (1988); G. Binasch, P. Grünberg, F.

Saurenbach, and W. Zinn, *Phys. Rev. B* **39**, 4828 (1989).

⁸J. C. Slonczewski, *J. Magn. Magn. Mater.* **159**, L1 (1996).

⁹J. A. Katine, F. J. Albert, R. A. Buhrman, E. B. Myers, and D. C. Ralph, *Phys. Rev. Lett.* **84**, 3149 (2000).

¹⁰C. Heide, P. E. Zilberman, and R. J. Elliott, *Phys. Rev. B* **63**, 064424 (2001).

¹¹K. Hathaway and E. Dan Dahlberg, *Am. J. Phys.* **75**, 871 (2007).

¹²T. Miller, A. Samsavar, G. E. Franklin, and T.-C. Chiang, *Phys. Rev. Lett.* **61**, 1404 (1988); K. Garrison, Y. Chang, and P. D. Johnson, *ibid.* **71**, 2801 (1993); C. Carbone, E. Vescovo, O. Rader, W. Gudat, and W. Eberhardt, *ibid.* **71**, 2805 (1993); B. A. Jones and C. B. Hanna, *ibid.* **71**, 4253 (1993); J. E. Ortega, F. J. Himpfel, G. J. Mankey, and R. F. Willis, *Phys. Rev. B* **47**, 1540 (1993).

¹³F. J. Himpfel, T. A. Jung, and P. F. Seidler, *IBM J. Res. Dev.* **42**, 33 (1998).

¹⁴I. Y. Popov and E. S. Tesovskaya, *Teor. Mat. Fiz.* **146**, 429 (2006) [*Theor. Math. Phys.* **146**, 361 (2006)]; L. V. Gortinskaya, I. Y. Popov, E. S. Tesovskaya, and V. M. Uzdin, *Physica E (Amsterdam)* **36**, 12 (2007).

¹⁵S. N. Okuno and K. Inomata, *Phys. Rev. Lett.* **72**, 1553 (1994).

¹⁶B. J. van Wees, H. van Houten, C. W. J. Beenakker, J. G. Will-

- iamson, L. P. Kouwenhoven, D. van der Marel, and C. T. Foxon, *Phys. Rev. Lett.* **60**, 848 (1988).
- ¹⁷D. A. Wharam, T. J. Thornton, R. Newbury, M. Pepper, H. Ahmed, J. E. F. Frost, D. G. Hasko, D. C. Peacock, D. A. Ritchie, and G. A. C. Jones, *J. Phys. C* **21**, L209 (1988).
- ¹⁸E. R. Johnson, M. Levitin, and L. Parnowski, *SIAM J. Math. Anal.* **37**, 1465 (2006).
- ¹⁹K. Davies, *Ionospheric Radio* (Peregrinus, London, 1991).
- ²⁰S. F. Mahmoud, *Electromagnetic Waveguides: Theory and Applications* (Peregrinus, London, 1991).
- ²¹J. Tworzyczo, B. Trauzettel, M. Titov, A. Rycerz, and C. W. J. Beenakker, *Phys. Rev. Lett.* **96**, 246802 (2006).
- ²²V. L. Ginsburg and L. D. Landau, *Zh. Eksp. Teor. Fiz.* **20**, 1064 (1950).
- ²³P. G. de Gennes, *Superconductivity of Metals and Alloys* (Benjamin, New York, 1966).
- ²⁴L. D. Landau and E. M. Lifshitz, *Statistical Physics* (Pergamon, New York, 1980), Pt. 2.
- ²⁵L. D. Landau and E. M. Lifshitz, *Quantum Mechanics (Non-Relativistic Theory)* (Pergamon, New York, 1977).
- ²⁶E. A. Andryushin, V. L. Ginzburg, and A. P. Silin, *Usp. Fiz. Nauk* **163**(9), 105 (1993) [*Phys. Usp.* **36**, 854 (1993)]; E. A. Andryushin, V. L. Ginzburg, and A. P. Silin, *Usp. Fiz. Nauk*, **163**(11), 102 (1993) [*Phys. Usp.* **36**, 1086 (1993)].
- ²⁷H. J. Fink and W. C. H. Joiner, *Phys. Rev. Lett.* **23**, 120 (1969).
- ²⁸R. Benoist and W. Zwerger, *Z. Phys. B: Condens. Matter* **103**, 377 (1997).
- ²⁹V. M. Fomin, V. R. Misko, J. T. Devreese, and V. V. Moshchalkov, *Phys. Rev. B* **58**, 11703 (1998).
- ³⁰V. M. Fomin, J. T. Devreese, and V. V. Moshchalkov, *Europhys. Lett.* **42**, 553 (1998).
- ³¹V. Bruyndoncx, L. Van Look, M. Verschuere, and V. V. Moshchalkov, *Phys. Rev. B* **60**, 10468 (1999).
- ³²L. F. Chibotaru, A. Ceulemans, M. Lorenzini, and V. V. Moshchalkov, *Europhys. Lett.* **63**, 159 (2003); **63**, 476 (2003).
- ³³A. F. Slachmuylders, B. Partoens, and F. M. Peeters, *Phys. Rev. B* **71**, 245405 (2005).
- ³⁴C. Carballeira, V. V. Moshchalkov, L. F. Chibotaru, and A. Ceulemans, *Phys. Rev. Lett.* **95**, 237003 (2005).
- ³⁵B. J. Baelus, B. Partoens, and F. M. Peeters, *Phys. Rev. B* **73**, 212503 (2006).
- ³⁶V. V. Moshchalkov, L. Gielen, C. Strunk, R. Jonckheere, X. Qiu, C. Van Haesendonck, and Y. Bruynseraede, *Nature (London)* **373**, 319 (1995).
- ³⁷L. F. Chibotaru, A. Ceulemans, V. Bruyndoncx, and V. V. Moshchalkov, *Nature (London)* **408**, 833 (2000).
- ³⁸M. Morelle, D. S. Golubović, and V. V. Moshchalkov, *Phys. Rev. B* **70**, 144528 (2004); L. F. Chibotaru, A. Ceulemans, M. Morelle, G. Teniers, C. Carballeira, and V. V. Moshchalkov, *J. Math. Phys.* **46**, 095108 (2005).
- ³⁹V. V. Moshchalkov, *J. Supercond. Novel Magn.* **19**, 409 (2006).
- ⁴⁰D. Saint-James and P. G. de Gennes, *Phys. Lett.* **7**, 306 (1963).
- ⁴¹R. D. Parks and J. M. Mochel, *Phys. Rev. Lett.* **11**, 354 (1963).
- ⁴²Y. Guo, Y.-F. Zhang, X.-Y. Bao, T.-Z. Han, Z. Tang, L.-X. Zhang, W.-G. Zhu, E. G. Wang, Q. Niu, Z. Q. Qiu, J.-F. Jia, Z.-X. Zhao, and Q.-K. Xue, *Science* **306**, 1915 (2004).
- ⁴³B.-H. Zhu, S.-P. Zhou, Y.-M. Shi, G.-Q. Zha, and K. Yang, *Phys. Rev. B* **74**, 014501 (2006).
- ⁴⁴M. Jouguet, *Ann. Telecommun.* **2**, 78 (1947); *Cables Transm.* **1**, 39 (1947).
- ⁴⁵C. P. Bates, *Bell Syst. Tech. J.* **49**, 2259 (1969).
- ⁴⁶P. Exner and P. Šeba, *J. Math. Phys.* **30**, 2574 (1989).
- ⁴⁷R. L. Schult, D. G. Ravenhall, and H. W. Wyld, *Phys. Rev. B* **39**, 5476 (1989).
- ⁴⁸J. Goldstone and R. L. Jaffe, *Phys. Rev. B* **45**, 14100 (1992).
- ⁴⁹J. P. Carini, J. T. Londergan, K. Mullen, and D. P. Murdock, *Phys. Rev. B* **46**, 15538 (1992); J. P. Carini, J. T. Londergan, K. Mullen, and D. P. Murdock, *ibid.* **48**, 4503 (1993); J. P. Carini, J. T. Londergan, D. P. Murdock, D. Trinkle, and C. S. Yung, *ibid.* **55**, 9842 (1997).
- ⁵⁰F. Sols and M. Macucci, *Phys. Rev. B* **41**, 11887 (1990).
- ⁵¹O. Olendski and L. Mikhailovska, *Phys. Rev. B* **66**, 035331 (2002).
- ⁵²J. Dittrich and J. Kříž, *J. Phys. A* **35**, L269 (2002).
- ⁵³O. Olendski and L. Mikhailovska, *Phys. Rev. E* **67**, 056625 (2003).
- ⁵⁴D. Krejčířk and J. Kříž, *Publ. Res. Inst. Math. Sci.* **41**, 757 (2005).
- ⁵⁵E. Montevecchi and J. O. Indekeu, *Europhys. Lett.* **51**, 661 (2000); *Phys. Rev. B* **62**, 14359 (2000).
- ⁵⁶C. Gorria, Y. B. Gaididei, M. P. Soerensen, P. L. Christiansen, and J. G. Caputo, *Phys. Rev. B* **69**, 134506 (2004).
- ⁵⁷D. R. Gulevich and F. V. Kusmartsev, *Phys. Rev. Lett.* **97**, 017004 (2006); *Supercond. Sci. Technol.* **20**, S60 (2007).
- ⁵⁸O. Olendski and L. Mikhailovska, *Phys. Rev. B* **72**, 235314 (2005).
- ⁵⁹H. Su and B.-Y. Gu, *Phys. Lett. A* **324**, 61 (2004).
- ⁶⁰A. F. Andreev, *Zh. Eksp. Teor. Fiz.* **46**, 1823 (1964)[*Sov. Phys. JETP* **19**, 1228 (1964)].
- ⁶¹R. L. Schult, H. W. Wyld, and D. G. Ravenhall, *Phys. Rev. B* **41**, 12760 (1990).
- ⁶²K. Vacek, H. Kasai, and A. Okiji, *J. Phys. Soc. Jpn.* **61**, 27 (1992); K. Vacek, A. Okiji, and H. Kasai, *Phys. Rev. B* **47**, 3695 (1993); K. Vacek, A. Okiji, and H. Kasai, *ibid.* **48**, 11412 (1993).
- ⁶³J. J. Palacios and C. Tejedor, *Phys. Rev. B* **48**, 5386 (1993).
- ⁶⁴K. Amemiya, *J. Phys. Soc. Jpn.* **68**, 567 (1999); K. Amemiya, *ibid.* **68**, 1464 (1999); K. Amemiya, *ibid.* **72**, 135 (2003).
- ⁶⁵O. Olendski and L. Mikhailovska, *J. Phys. A* **40**, 4609 (2007).
- ⁶⁶J. C. P. Miller, *Tables of Weber Parabolic Cylinder Functions* (Her Majesty's Stationery Office, London, 1955); I. E. Kireeva and K. A. Karpov, *Tables of Weber Functions* (Pergamon, Oxford, 1961); H. Bateman and A. Erdélyi, *Higher Transcendental Functions* (McGraw-Hill, New York, 1953), Vol. 2.
- ⁶⁷*Handbook of Mathematical Functions*, edited by M. Abramowitz and I. A. Stegun (Dover, New York, 1964).
- ⁶⁸E. Butkov, *Mathematical Physics* (Addison-Wesley, New York, 1968).
- ⁶⁹R. Landauer, *IBM J. Res. Dev.* **1**, 223 (1957); **32**, 306 (1988); **21**, 863 (1970).
- ⁷⁰H. J. Fink and A. G. Presson, *Phys. Rev.* **151**, 219 (1966); **155**, 566 (1967); H. J. Fink and A. G. Presson, *ibid.* **168**, 399 (1968).
- ⁷¹N. C. Constantinou, M. Masale, and D. R. Tilley, *J. Phys.: Condens. Matter* **4**, L293 (1992); M. Masale, N. C. Constantinou, and D. R. Tilley, *Supercond. Sci. Technol.* **6**, 287 (1993); M. Masale, *Physica C* **377**, 75 (2002).
- ⁷²A. I. Buzdin, *Phys. Rev. B* **47**, 11416 (1993); A. Bezryadin, A. Buzdin, and B. Pannetier, *Phys. Lett. A* **195**, 373 (1994).
- ⁷³V. V. Moshchalkov, X. G. Qiu, and V. Bruyndoncx, *Phys. Rev. B* **55**, 11793 (1997).

- ⁷⁴P. S. Deo, V. A. Schweigert, F. M. Peeters, and A. K. Geim, Phys. Rev. Lett. **79**, 4653 (1997).
- ⁷⁵W. V. Pogosov, Phys. Rev. B **65**, 224511 (2002).
- ⁷⁶G.-Q. Zha, S.-P. Zhou, B.-H. Zhu, and Y.-M. Shi, Phys. Rev. B **73**, 104508 (2006); G.-Q. Zha, S.-P. Zhou, B.-H. Zhu, Y.-M. Shi, and H.-W. Zhao, *ibid.* **74**, 024527 (2006).
- ⁷⁷M. Büttiker, Phys. Rev. B **38**, 9375 (1988).
- ⁷⁸B. I. Halperin, Phys. Rev. B **25**, 2185 (1982).
- ⁷⁹M. Robnik, J. Phys. A **19**, 3619 (1986).
- ⁸⁰T.-L. Ho, Phys. Rev. B **50**, 4524 (1994).
- ⁸¹M. Grayson, M. Huber, M. Rother, W. Biberacher, W. Wegscheider, M. Bichler, and G. Abstreiter, Physica E (Amsterdam) **25**, 212 (2004); M. Huber, M. Grayson, M. Rother, W. Biberacher, W. Wegscheider, and G. Abstreiter, Phys. Rev. Lett. **94**, 016805 (2005); M. Grayson, L. Steinke, M. Huber, D. Schuh, M. Bichler, and G. Abstreiter, Phys. Status Solidi B **245**, 356 (2008).
- ⁸²E. Simánek, Phys. Rev. B **59**, 10152 (1999).
- ⁸³J. U. Nöckel, Phys. Rev. B **46**, 15348 (1992).
- ⁸⁴P. Freitas and D. Krejčířk, Math. Phys., Anal. Geom. **9**, 335 (2006).
- ⁸⁵Y. K. Kato, R. C. Myers, A. C. Gossard, and D. D. Awschalom, Appl. Phys. Lett. **87**, 022503 (2005).
- ⁸⁶M. Grayson, D. Schuh, M. Bichler, M. Huber, G. Abstreiter, L. Hoepfel, J. Smet, and K. von Klitzing, Physica E (Amsterdam) **22**, 181 (2004); M. Grayson, D. Schuh, M. Huber, M. Bichler, and G. Abstreiter, Appl. Phys. Lett. **86**, 032101 (2005); M. Grayson, L. Steinke, D. Schuh, M. Bichler, L. Hoepfel, J. Smet, K. v. Klitzing, D. K. Maude, and G. Abstreiter, Phys. Rev. B **76**, 201304(R) (2007).
- ⁸⁷I. V. Grigorieva, A. K. Geim, S. V. Dubonos, K. S. Novoselov, D. Y. Vodolazov, F. M. Peeters, P. H. Kes, and M. Hesselberth, Phys. Rev. Lett. **92**, 237001 (2004).
- ⁸⁸L. P. Gor'kov, Zh. Eksp. Teor. Fiz. **36**, 1918 (1959) [Sov. Phys. JETP **9**, 1364 (1959)].
- ⁸⁹A. K. Geim, I. V. Grigorieva, S. V. Dubonos, J. G. S. Lok, J. C. Maan, A. E. Filippov, and F. M. Peeters, Nature (London) **390**, 259 (1997).